Peer-reviewed version available at Energies 2017, 10, 1828; doi:10.3390/en10111828

# Numerical Investigation on Flow and Heat Transfer Characteristics of Supercritical Liquefied Natural Gas in an Airfoil Fin Printed Circuit Heat Exchanger

**Zhongchao Zhao *, Kai Zhao, Dandan Jia, Pengpeng Jiang and Rendong Shen**

School of Energy and Power, Jiangsu University of Science and Technology, Jiangsu China

* Corresponding author: E-mail address: zhongchaozhao@just.edu.cn; Tel.: +86-0511-84493050

**Abstract:** As a new kind of highly compact and efficient micro-channel heat exchanger, printed circuit heat exchanger (PCHE) is a promising candidate satisfying the heat exchange requirements of liquefied natural gas (LNG) vaporization at low and high pressure. The effects of airfoil fin arrangement on heat transfer and flow resistance were numerically investigated using supercritical liquefied natural gas (LNG) as working fluid. The thermal properties of supercritical LNG were tested by utilizing REFPROF software database. Numerical simulation was performed using FLUENT. The inlet temperature of supercritical LNG was 121 K, and its pressure was 10.5MPa. The reference mass flow rate of LNG was set as 1.22 g/s for the vertical pitch $L_v$ = 1.67 mm and the staggered pitch $L_s$ = 0 mm, with the Reynolds number of about 3750. The SST k-ω model with enhanced wall treatment was selected by comparing with the experimental data. The airfoil fin PCHE had better thermal-hydraulic performance than that of the straight channel PCHE. Moreover, the airfoil fins with staggered arrangement displayed better thermal performance than that of the fins with parallel arrangement. The thermal-hydraulic performance of airfoil fin PCHE was improved with increasing $L_s$ and $L_v$. Moreover, $L_v$ affected the Nusselt number and pressure drop of airfoil fin PCHE more obviously. In conclusion, a sparser staggered arrangement of fins showed a better thermal-hydraulic performance in airfoil fin PCHE.

**Keyword:** printed circuit heat exchanger; airfoil fin; supercritical LNG; thermal-hydraulic performance

## 1. Introduction

Owing to high calorific value and low carbon dioxide emissions, natural gas (NG) has become the best choice for substituting traditional resources such as coal and petroleum [1,2]. Generally, NG is cooled to liquefied natural gas (LNG), allowing it to be stored and transported for long distance. LNG is then heated and regasified to NG before being transmitted into the pipeline to meet the demand of users [3,4]. As critical equipment in LNG gasification system, efficient and reliable vaporization devices have been spotlighted. Four kinds of LNG vaporizers are mainly commercially available: intermediate fluid vaporizer, open rack vaporizer (ORV), super ORV, and submerged combustion vaporizer[5-7].

However, traditional LNG vaporizers cannot meet the requirements of miniaturization

and high compactness in the construction of LNG gasification system[8]. Therefore, it is urgent to find an efficient and compact heat exchanger to replace these traditional vaporizers. Because of safety, high compactness and efficiency, printed circuit heat exchanger(PCHE) has drawn wide attention in these years[9-12]. PCHE is a micro-channel heat exchanger manufactured by photochemical etching and diffusion bonding [13-16]. As a result, PCHE shows better heat transfer performance than those of other types of heat exchanger due to larger heat surface area caused by many micro-channels. Nevertheless, PCHE suffers from enhanced pressure drop. Therefore, researchers have endeavored to improve the thermal-hydraulic characteristics of PCHE[17-24].

Four types of PCHE flow channels, i.e. straight, zigzag, S-shape, and airfoil fin,have been developed so far. Mylavarapu et al. [25] experimentally tested PCHE with straight, circular and semicircular channels at 2.7 MPa with various Reynolds numbers. The transition from laminar flow to flow regime occurred much earlier in the semicircular channel than within the circular pipe.

Ma et al. [26] studied the pressure drop mechanism and the local heat transfer of PCHE with zigzag channel and the effect of inclined angle of channel on the thermal-hydraulic performance of PCHE under the operating condition of very high temperature reactor. Figley et al. [27] studied the heat transfer and pressure drop characteristics of PCHE with zigzag channel by the aid of three-dimensional numerical simulations. Aneesh et al.[28] studied thermal-hydraulic characteristics and property of 3D straight channel based PCHE. Khan et al. [29] investigated the thermal-hydraulic characteristics and performance of PCHE for various angles of bend (θ=0°,5°,10°,and 15°) and different Reynolds numbers (Re = 350, 700, 1400 and 2100). With increasing Re and θ, the thermal hydraulic performance was boosted.

PCHEs with straight and Z-shaped channels were analyzed initially. However, many researchers found that PCHEs with distributed fins, such as S-shaped fins and airfoil fins, had better thermal-hydraulic characteristics. Ngo et al. [30] studied a new PCHE with an S-shaped fin structure applied to a hot water supplier which takes the supercritical $CO_2$ as heat source. And the new PCHE had about 3.3 times less volume, but lower pressure drop by 37% in $CO_2$ side and by ten times in $H_2O$ side than existing 1.5 MW/m$^3$ hot water supplier.

Kim et al. [31] proposed an airfoil fin, making the pressure drop of the airfoil fin one-twentieth of that of zigzag channel but their total heat transfer rates per unit volume were basically the same, to enhance the thermal hydraulic performance of PCHE. Although PCHE has better thermal hydraulic performance than those of traditional heat exchangers due to the smaller hydraulic diameter of flow channel, it also raises the pressure drop. In addition to optimizing the channel shape of PCHE, many researchers have focused on the fluid in flow channels[32]. Compared to traditional fluids, supercritical fluid has many advantageous characteristics as the working fluid in PCHE, such as high density, low viscosity and high thermal conductivity [33-35].

Supercritical carbon dioxide and water have been applied in PCHE. Kruizenga et al. [36] performed an experimental study to estimate the pressure drop and heat transfer of PCHE which the supercritical $CO_2$ was selected as the working fluid. The heat transfer significantly increased when the pseudo critical temperature and critical pressure were approached.

Kim et al. [37] performed numerical investigations to study the performance of airfoil fin PCHE which supercritical carbon dioxide were used as the working fluid. They examined the

optimal arrangement of airfoil fins with an objective function, and the arrangement had a staggered number of 1 mm.

Regardless of extensive studies on the thermal hydraulic performance of PCHEs using supercritical carbon dioxide and water as working fluids, the thermal-hydraulic performance of PCHE used in an LNG vaporization system at low temperature and high pressure has rarely been reported hitherto. In this study, the numerical simulation method was used to analyze the thermal-hydraulic performance of PCHE using supercritical LNG as the work fluid. The heat transfer and flow characteristics of supercritical LNG in a single channel of straight channel PCHE and airfoil fin PCHE were compared at different mass fluxes. To obtain the correlations between performance factors and configuration factors, pressure drop and heat transfer were replaced with dimensionless representations (Nusselt number and Euler number). The effects of airfoil fin arrangements on heat transfer and pressure drop characteristics were analyzed. Finally, an optimal design for the fin arrangement in an airfoil fin PCHE was suggested. The results in favour of the optimum thermal design and operation of high-performance airfoil fin PCHE.

## 2. Computational Fluid Dynamic Analysis for thermal-hydraulic performance

### *2.1 Thermal-physical properties of supercritical LNG*

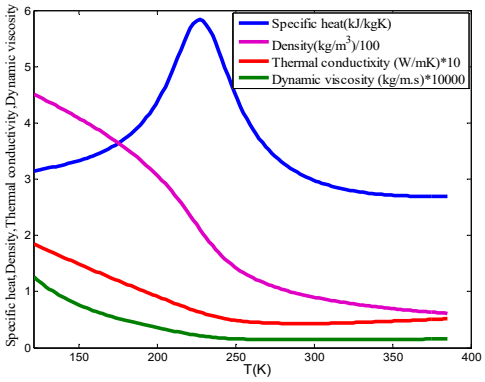


**Fig.1.** Thermal-physical properties of LNG at 10.5 MPa

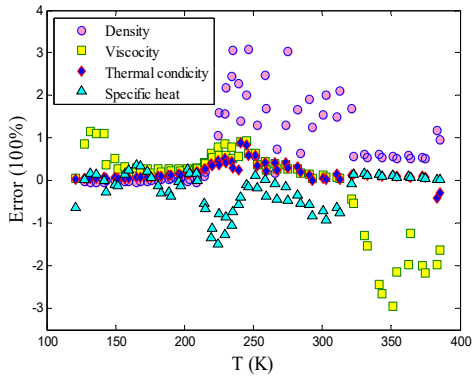


**Fig.2.** Error curve of linear interpolation function

In this study, the LNG pressure was 10.5 MPa, exceeding its critical pressure (P=4.59 MPa). As a result, LNG in the PCHE channel was in the supercritical state, where obvious liquid phase

Preprints (www.preprints.org) | NOT PEER-REVIEWED | Posted: 12 October 2017 doi:10.20944/preprints201710.0078.v1

Peer-reviewed version available at Energies 2017, 10, 1828; doi:10.3390/en10111828

and gas phase did not exist. Like other supercritical fluids, supercritical LNG also has various favorable characteristics like high density, high thermal conductivity and low viscosity. The properties including density, thermal conductivity, specific heat and viscosity were calculated by REFPROP 9.0 software (Fig.1). Meanwhile, the accuracy of the property data in the entire regime computation was validated (Fig.2). The errors were within ±4%, indicating the viability of this computation method. The thermal properties of supercritical LNG were calculated with the FLUENT software by defining the piecewise-linear functions of temperature (Table 1).

**Table1.** Property correlations of LNG at 10.5 MPa

| |
|---|
| **(1) 121-227 K** |
| $\rho=8256.5933-285.3922T+4.3559T^2-0.035267T^3+1.5894\times10^{-4}T^4-3.7784\times10^{-7}T^5+3.6917\times10^{-10}T^6$ |
| $C_p=-1.0199\times10^6+3.8183\times10^4T-589.1061T^2+4.8079T^3-0.02189T^4+5.28734\times10^{-5}T^5-5.23296\times10^{-8}T^6$ |
| $\lambda=1.6663-0.051726T+7.9379\times10^{-4}T^2-6.6085\times10^{-6}T^3+3.0653\times10^{-8}T^4-7.4993\times10^{-11}T^5+7.5617\times10^{-14}T^6$ |
| $\mu=4.0977\times10^{-3}-1.2117\times10^{-4}T+1.5988\times10^{-6}T^2-1.1623\times10^{-8}T^3+4.8332\times10^{-11}T^4-1.0811\times10^{-13}T^5+1.01103\times10^{-16}T^6$ |
| **(2) 227-315 K** |
| $\rho=-3.89476+7.7791\times10^3T-63.6984T^2+0.273703T^3-6.4991\times10^{-4}T^4+8.06233\times10^{-7}T^5-4.06261\times10^{-10}T^6$ |
| $C_p=-4.48732\times10^7+9.7441\times10^5T-8.78917\times10^3T^2+42.17166T^3-0.011355T^4+1.62727\times10^{-4}T^5-9.6971\times10^{-8}T^6$ |
| $\lambda=-99.92683+2.24495T-0.0208241T^2+1.02288\times10^{-4}T^3-2.8093\times10^{-7}T^4+4.09353\times10^{-10}T^5-2.47389\times10^{-13}T^6$ |
| $\mu=1.58763\times10^{-2}+3.9445\times10^{-4}T-3.96736\times10^{-6}T^2+2.08564\times10^{-8}T^3-6.07355\times10^{-11}T^4+9.3195\times10^{-14}T^5-5.8999\times10^{-17}T^6$ |
| **(3) 315-385 K** |
| $\rho=9403.1676-140.8996T+0.90485T^2-3.14226\times10^{-3}T^3+6.19397\times10^{-6}T^4-6.55485\times10^{-9}T^5+2.905\times10^{-12}T^6$ |
| $C_p=-4.28439\times10^5-6.56712\times10^3T+42.6554T^2-0.14901T^3+2.94672\times10^{-4}T^4-3.12279\times10^{-7}T^5+1.383995\times10^{-10}T^6$ |
| $\lambda=2.2909-0.03353T+2.35313\times10^{-4}T^2-8.3695\times10^{-7}T^3+1.68679\times10^{-9}T^4-1.8217\times10^{-12}T^5+8.22556\times10^{-16}T^6$ |
| $\mu=4.92979\times10^{-3}-8.37086\times10^{-5}T+5.94466\times10^{-7}T^2-2.25336\times10^{-9}T^3+4.8073\times10^{-12}T^4-5.47099\times10^{-15}T^5+2.5942\times10^{-18}T^6$ |

*2.2 Physical models and definition of airfoil fin arrangement parameters*

Generally, an airfoil fin PCHE consists of several micro-channels, including several airfoil fins in one channel. Therefore, it is extremely difficult to simulate the entire heat exchanger geometry because a powerful computer and long computation time are needed. However, as shown in Fig.3, the flow channel formed by airfoil fins is periodic in both longitudinal direction and transverse direction, except for the plate border in a PCHE. Therefore, considering the computing resource, forty periodic fin structures along the flow direction from the core area of heat exchanger with the length of 260 mm were selected firstly. The vertical pitch $L_v$ and staggered pitch $L_s$ of airfoil fins were 1.67 mm and 0 mm respectively, aiming to compare the

Preprints (www.preprints.org) | NOT PEER-REVIEWED | Posted: 12 October 2017 doi:10.20944/preprints201710.0078.v1

Peer-reviewed version available at Energies 2017, 10, 1828; doi:10.3390/en10111828

heat transfer and flow characteristics of supercritical LNG between airfoil fin and straight channel with the same channel length and hydraulic diameter. The numerical models of straight channel and airfoil fin are shown in Fig.4 and Fig.5 respectively.

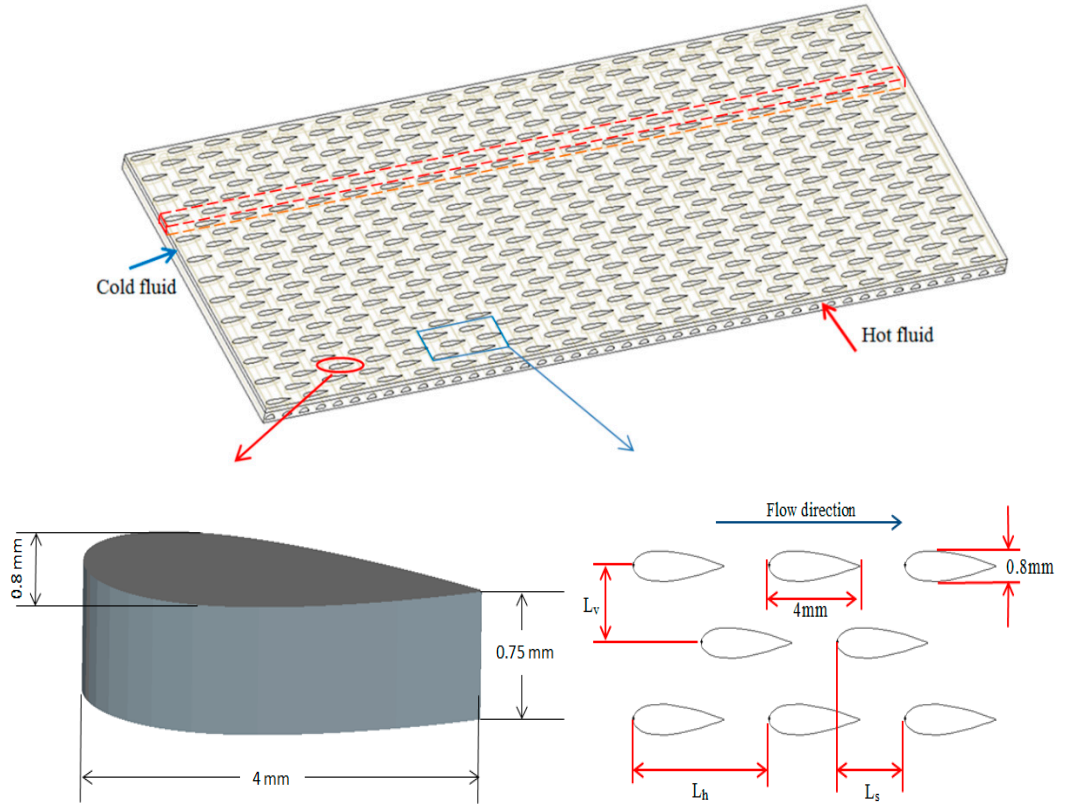


**Fig.3.** Schematic diagram of internal core structure of airfoil fin PCHE

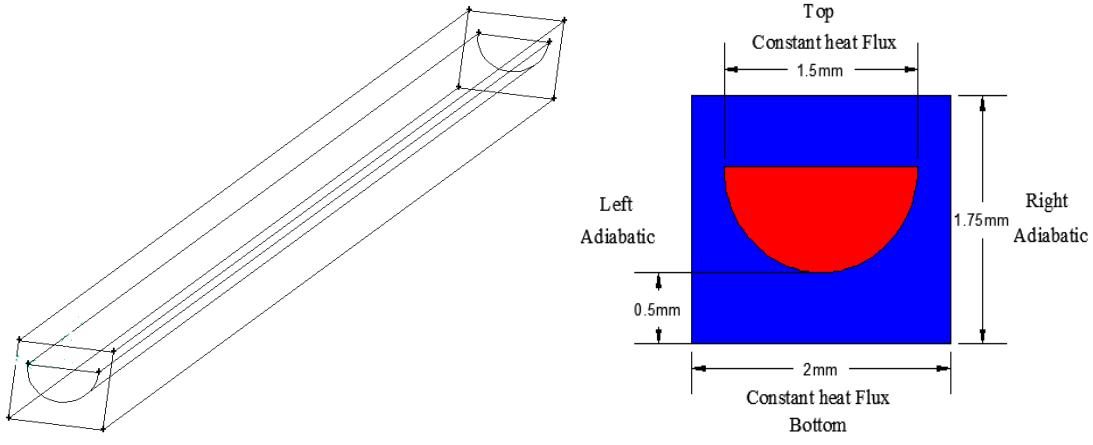


**(a)** **(b)**

**Fig.4.** Schematic diagram of (a) Straight channel geometric model and (b) cross-section of straight channel

Then, to study the effects of airfoil fin arrangements on the flow and heat transfer characteristics of supercritical LNG, six periodic fin structures along the flow direction and three along the transverse direction were selected as the simulation domain. The airfoil fin

Preprints (www.preprints.org) | NOT PEER-REVIEWED | Posted: 12 October 2017 doi:10.20944/preprints201710.0078.v1

Peer-reviewed version available at Energies 2017, 10, 1828; doi:10.3390/en10111828

PCHE have three important geometric parameters (Fig.3). The separation distance of staggered arrangement is presented by $L_s$. There is a periodicity between un-staggered arrangement and fully staggered arrangement. $L_h$ indicates the separation distance between one airfoil head and adjacent airfoil head in a row. The separation distance between one row and adjacent row in the vertical direction is indicated by $L_v$. Herein, $L_h$ was 6 mm, $L_s$ varied from 0 to 4 mm and $L_v$ changed from 1.3 mm to 3 mm. According to the configuration, the width (W) of the heat transfer region of the entire domain varied from 3.9 mm to 9 mm. The vertical pitch $L_v$ = 1.67 mm and staggered pitch $L_s$ = 0 mm were selected as the baseline model.

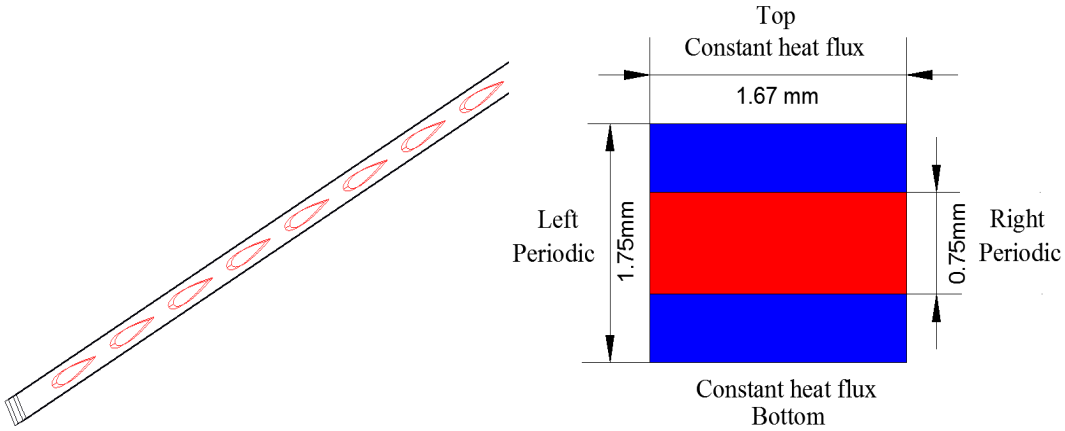


**Fig.5.** Schematic diagram of (a) the airfoil fin channel geometric model and (b) cross-section of airfoil fin channel

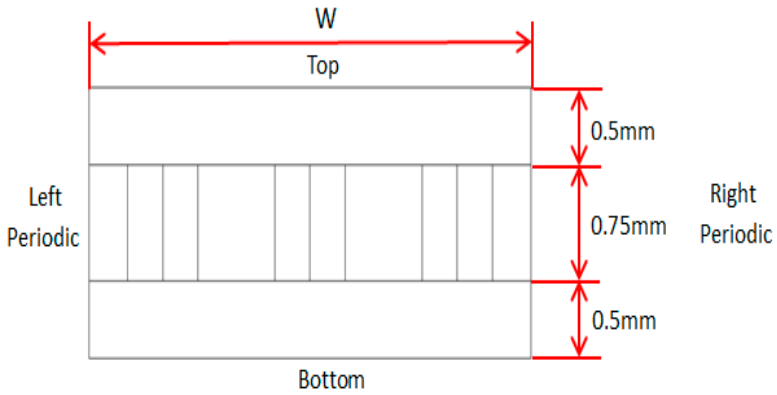


**Fig.6.** Schematic diagram of airfoil fin PCHE

A schematic diagram of the simulation domain showed (Fig.7) that $L_v$ = 1.67 mm and $L_s$ = 0 mm. The working fluid was supercritical LNG, and the material of substrate plates and fins was steel. The mass flux inlet was applied for the inlet boundary condition of the simulation domain, and the inlet temperature and reference mass flux were set at 121 K and 325 kg/m$^2$·s respectively. The outlet boundary condition was set as pressure outlet. As shown in Figure 6, a periodic boundary condition in the left/right positions, as well as a constant heat flux applied to the top and bottom positions is 58713.75W/m$^2$.

Preprints (www.preprints.org) | NOT PEER-REVIEWED | Posted: 12 October 2017 doi:10.20944/preprints201710.0078.v1

Peer-reviewed version available at Energies 2017, 10, 1828; doi:10.3390/en10111828

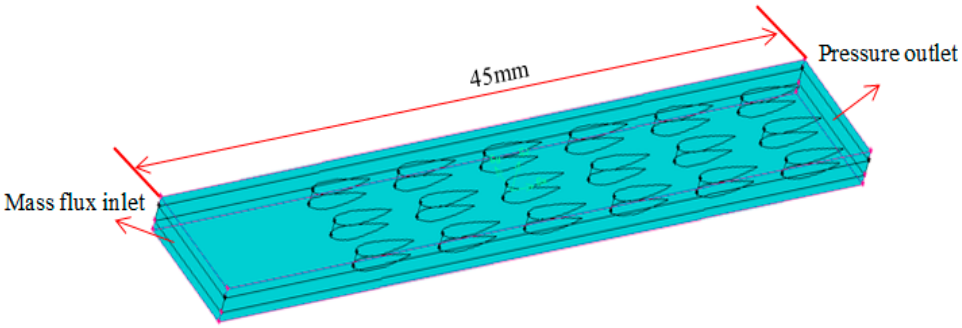


**Fig.7.** 3D view of computational domain for airfoil fin PCHE

*2.3 Numerical method and grid independence*

ANSYS Fluent 14.5 was used for numerical evaluation of the airfoil fin PCHE. The set mass flow rate corresponded to turbulent flow regimes in the PCHE cold channels. It is important to select a proper turbulence model for numerical calculations. Kim and No [11] reported that the shear stress transport k-ω model (SST k-ω) [12] extremely well predicted a fine grid near the wall in supercritical calculation. Therefore, the SST k-ω model was used in this study. The semi implicit method pressure linked equation algorithm was used to resolve the coupling of velocity and pressure. Before solution convergence, the residual for every variable was required to be less than $10^{-6}$. Meanwhile, the second order upwind, which has a smaller truncation error than that of the first order upwind, was used in the momentum equation and energy equation to ensure the accuracy of simulation.

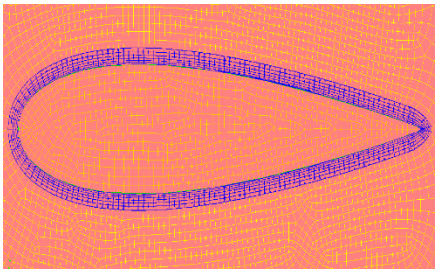

**Fig.8.** Top view of selected grid system

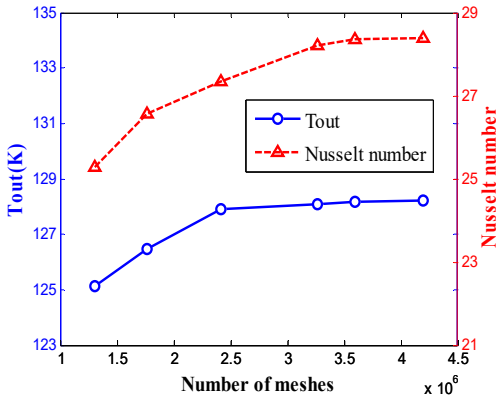


**Fig.9.** Dependency test of number of meshes

The structured computation mesh was generated by GAMBIT. The number of meshes was different for all cases on account of various dimensions of the simulation domain, so the model with staggered number $L_s = 0$ mm and vertical number $L_v = 1.67$ mm was selected as the baseline model. The mesh dependence test dominated the density of meshes(Fig.9). The influence of grid density on the accuracy of calculated results was studied by comparing six sets of grid numbers: 1302567, 1762753, 2415689, 3269854, 3594425 and 4196856 cells. By comparing the outlet temperature and Nusselt number, the optimal grid of 3594422 was selected considering the accuracy and computational efficiency. As shown in Fig.8, the grids are encrypted near the wall surfaces of fins and substrate plates to ensure that $y^+$ is lower than 1. Six boundary layers were established near the top and bottom walls and fin surfaces because of the strict

Preprints (www.preprints.org) | NOT PEER-REVIEWED | Posted: 12 October 2017 doi:10.20944/preprints201710.0078.v1

Peer-reviewed version available at Energies 2017, 10, 1828; doi:10.3390/en10111828

requirements for boundary grid in the supercritical flow and heat transfer, and the thickness of the first boundary layer was 0.01 mm.

*2.4 Model validation*

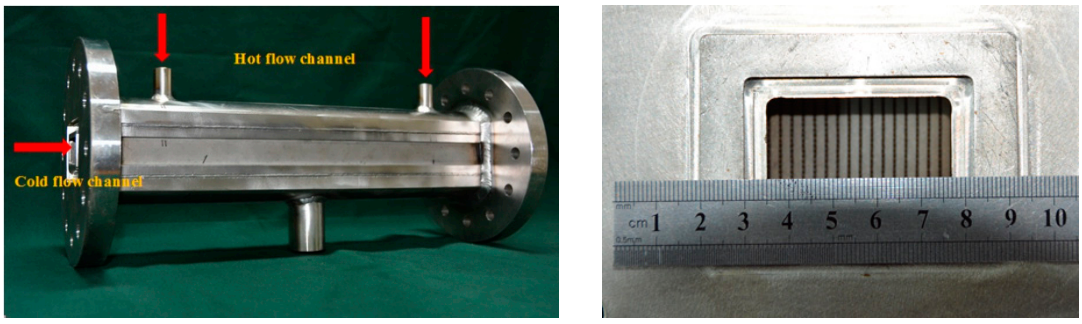


**(a)** **(b)**

**Fig.10.** (a) Tested airfoil fin PCHE and (b) cold channel of airfoil fin PCHE

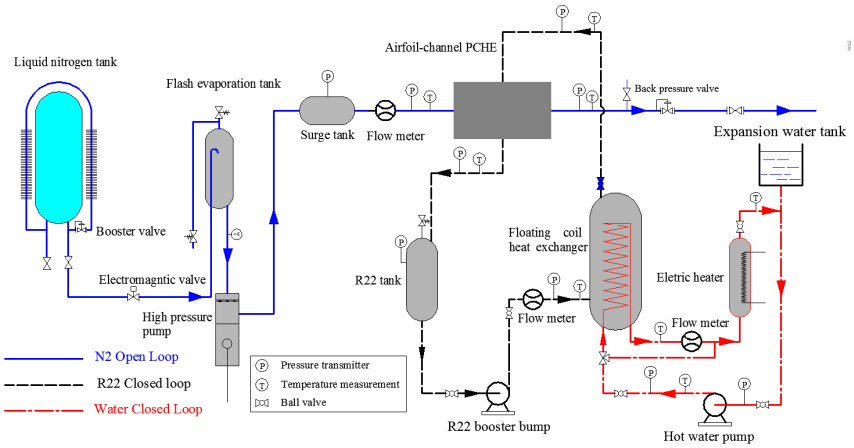


**(a)**

**(b)**

**Fig.11.** Experimental system with airfoil fin PCHE of (a) Schematic diagram of experimental set-up and (b) Photo of experimental system

In the present study, the heat transfer and flow characteristics of supercritical LNG in PCHE were investigated numerically. The results of CFD analysis should be compared with the

Preprints (www.preprints.org) | NOT PEER-REVIEWED | Posted: 12 October 2017 doi:10.20944/preprints201710.0078.v1

Peer-reviewed version available at Energies 2017, 10, 1828; doi:10.3390/en10111828

experimental data for validating analysis methodology. However, due to the flammable and explosive properties of LNG when the gas leaks or ventilation is insufficient at high pressure, supercritical nitrogen was selected to substitute LNG as the cold fluid. A crossflow PCHE with airfoil fin channels on the cold side and straight channels on the hot side was manufactured using stainless steel 316L (Fig.10). The airfoil fin with the chord length of 4 mm and the maximum thickness of 0.8 mm was selected. A experimental system was established to study the thermal-hydraulic performance of airfoil fin PCHE using supercritical nitrogen as the cold fluid and R22 as the hot fluid (Fig.11). The inlet temperature of nitrogen was 102 K when its pressure was varied from 5.5 MPa to 7.5 MPa. The mass flux of nitrogen varied from 233 to 421 kg/m$^2$·s, corresponding to turbulent flow regimes on the cold side of airfoil fin PCHE. In short, this PCHE had a good heat transfer ability at high pressure and low temperature. The overall heat transfer coefficient of this PCHE ranged from 850 to 2600 W/m$^2$K, and the heat transfer efficiency was up to approximately 98%.

Fig.10 displays the schematic diagram for the internal core structure of airfoil fin PCHE. It is rather complex to simulate the heat transfer processes of the total tested airfoil fin PCHE, and this study focused on the heat transfer and flow performance of cold fluid. Therefore, a single airfoil fin channel of cold side with full length (400 mm) which used supercritical nitrogen as the working fluid was selected to simulate and to compare with the experimental data (Fig.3). The numerical model of this section was the same as that in Fig.5, except for the length. The inlet temperature of nitrogen was 102 K when its pressure was varied from 5.5 MPa to 7.5 MPa. The mass flux of nitrogen was 421 kg/m$^2$·s, corresponding to turbulent flow regimes on the cold side of airfoil fin PCHE. The differences in the pressure drop and outlet temperature of the cold side between the numerical solutions and the experimental data were compared using Eq. 1.

$$Error = \frac{CFD - Experiment}{Experiment} \times 100\% \quad (1)$$

The pressure drop differences between the experimental and simulation results were analyzed when the mass flux was 421 kg/m$^2$·s (Table 2). The numerical results differed from the experimental data by 6.9% on average and by 11.62% at maximum. The deviation may be attributed to the inlet and outlet header pressure drop, as well as the uncertainty of pressure transmitters. Besides, the difference between numerical and experimental outlet temperatures on the cold side had an average error of 0.735% and the maximum difference of 1.127%. Therefore, the numerical data were in fairly good agreement with the experimental data, and the numerical model and method used herein were reliable.

**Table 2 .**Comparisons of simulation and experiment results

| Pressure (MPa) | Experiment results of □p/l (Pa/m) | Simulation results of □p/l (Pa/m) | Error (%) | Experiment results of $T_{out}$ (K) | Simulation results of $T_{out}$ (K) | Error (%) |
|---|---|---|---|---|---|---|
| 5.5 | 37090.61172 | 35226.12 | 5.03% | 279.45 | 278.13 | 0.472% |
| 6 | 33988.7737 | 32023.7 | 5.78% | 281.15 | 281.96 | 0.288% |
| 6.5 | 25650.67624 | 27635.15 | 7.74% | 282.55 | 283.67 | 1.12% |

Preprints (www.preprints.org) | NOT PEER-REVIEWED | Posted: 12 October 2017 doi:10.20944/preprints201710.0078.v1

Peer-reviewed version available at Energies 2017, 10, 1828; doi:10.3390/en10111828

| | | | | | | |
|---|---|---|---|---|---|---|
| 7 | 24175.74669 | 26985.37 | 11.62% | 284.35 | 285.96 | 0.669% |
| 7.5 | 23834.30936 | 24865.35 | 4.33% | 285.65 | 288.87 | 1.127% |

However, Fig.1 shows that the physical properties of supercritical fluid change substantially with rising temperature during heat transfer. The local heat transfer and flow characteristics of supercritical fluid cannot be obtained in the experimental apparatus. Therefore, the local parameters of airfoil fin PCHE were obtained through numerical simulation.

## 3. Objective function parameters

As a characteristic length of channel, hydraulic diameter $D_h$ is an important value in dimensionless analysis. It is defined as four times the cross-sectional area over a perimeter in the straight channel. Owing to the continual changes of cross-sectional area and perimeter, the hydraulic diameter cannot be the same as that of straight channel. Nevertheless, the placement of airfoil fin in Fig.3 is periodic. Therefore, the hydraulic diameter can be defined as equations below [38].

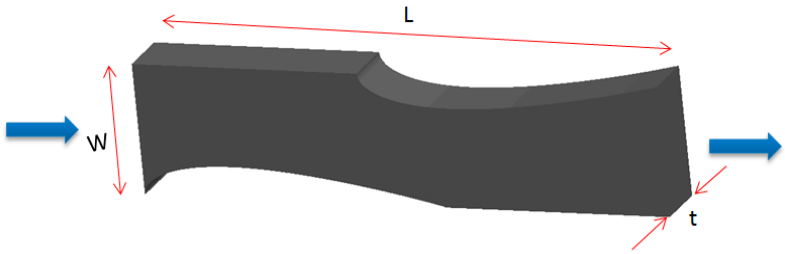


**Fig. 12.** Schematic diagram for calculation of hydraulic diameter

$$V = (LW - S_a)t \tag{2}$$

$$S = 2(\frac{P_a t}{2}) + 2(L - L_c)t + 2(WL - S_a) \tag{3}$$

$$D_h = 4V / S \tag{4}$$

where Sa is the top area of airfoil fin, and Pa is the perimeter of airfoil fin. V and S indicate the volume and side surface area of flow channel, respectively.

The convective heat transfer coefficient can be obtained by the following equation:

$$h = \frac{q_w}{T_{wall} - T_b} = \frac{q_w}{T_{wall} - (T_{out} + T_{in}) / 2} \tag{5}$$

where $q_w$ is the area-averaged wall heat flux, $T_{wall}$ is the area-average wall temperature, and $T_{in}$, $T_{out}$ and $T_b$ are the inlet, outlet and bulk temperatures of LNG obtained from the Fluent data respectively.

The Nusselt number is defined below:

$$Nu = \frac{hD_h}{\lambda} \tag{6}$$

where $D_h$ is the channel hydraulic diameter, and $\lambda$ is the thermal conductivity of LNG.

The Reynolds number can be calculated by Eq. 7.

$$\mathrm{Re} = \frac{\upsilon \rho D_h}{\mu} \tag{7}$$

where $D_h$ is the channel hydraulic diameter, $\rho$ is the density of LNG and $\mu$ is the dynamic viscosity of LNG.

The friction and acceleration effects caused by the density difference between inlet and outlet can result in the pressure drop.

$$\Delta P = \Delta P_{acc} + \Delta P_{fric} \tag{8}$$

$$\Delta P_{acc} = G^2\left(\frac{1}{\rho_{out}} - \frac{1}{\rho_{in}}\right) \tag{9}$$

$$\Delta P_{fric} = \frac{2 f L_u \rho \upsilon^2}{D_h} \tag{10}$$

where $\Delta P$ is the total pressure drop, $\Delta P_{acc}$ is the acceleration pressure drop and $\Delta P_{fric}$ is the friction pressure drop.

The Fanning friction factor f is defined below:

$$f = \frac{\tau_w}{\frac{1}{2}\rho u_m^2} \tag{11}$$

where $\tau_w$ is the wall shear stress.

In terms of pressure drop, the Euler number was selected as a representative pressure loss coefficient in this study. It reflects the relationship between pressure drop and dynamic velocity head, as well as the relative momentum loss rate.

$$Eu = \frac{\Delta P}{\rho u^2 / 2} \tag{12}$$

## 4. Results and discussion

### *4.1 Comparison of straight channel PCHE and airfoil fin PCHE*

In the present study, the heat transfer and flow characteristics of supercritical LNG in straight channel PCHE and airfoil fin PCHE with the same hydraulic diameter ($D_h$ = 0.917 mm) were numerically investigated. Fig.13 shows the velocity contours of supercritical LNG in airfoil fin and straight channel PCHEs when the mass flux is 325 kg/m²•s. When supercritical LNG was gradually heated, the bulk velocity significantly increased because of reduced density. However, the velocity increased rapidly in airfoil fin channel owing to continuous expansion and contraction in the sectional area of flow channel. The maximum velocity in the narrowest flow channel was nearly 3 times that in the inlet. Therefore, airfoil fins evidently disturbed

Preprints (www.preprints.org) | NOT PEER-REVIEWED | Posted: 12 October 2017 doi:10.20944/preprints201710.0078.v1

Peer-reviewed version available at Energies 2017, 10, 1828; doi:10.3390/en10111828

supercritical LNG, which increased heat transfer and flow resistance simultaneously.

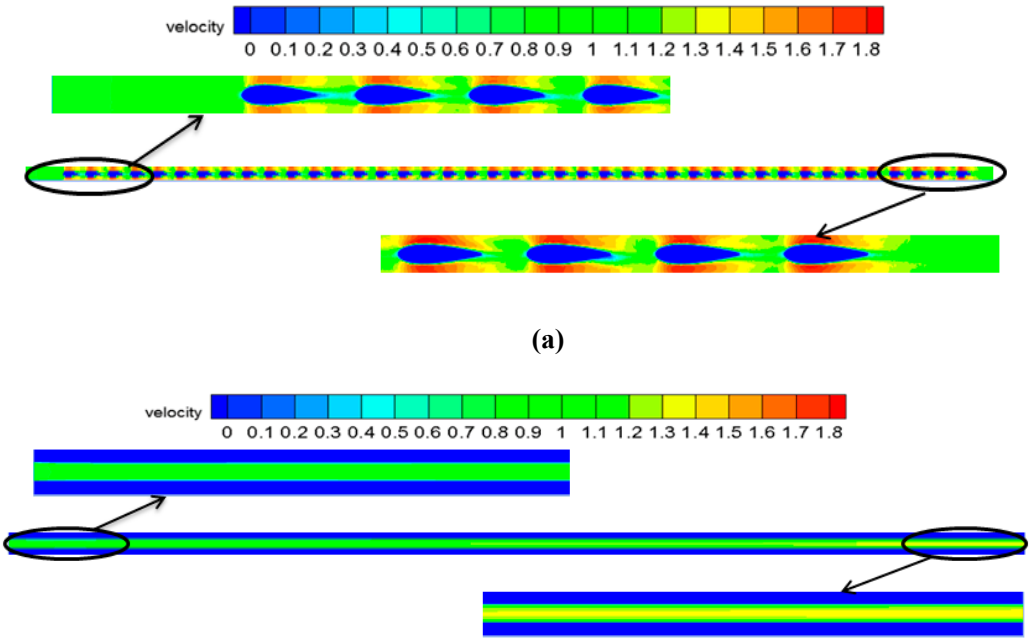


**Fig.13.**(a)Plots of velocity contours in airfoil fin channel and (b)straight channel when mass flux is 325 kg/m²•s

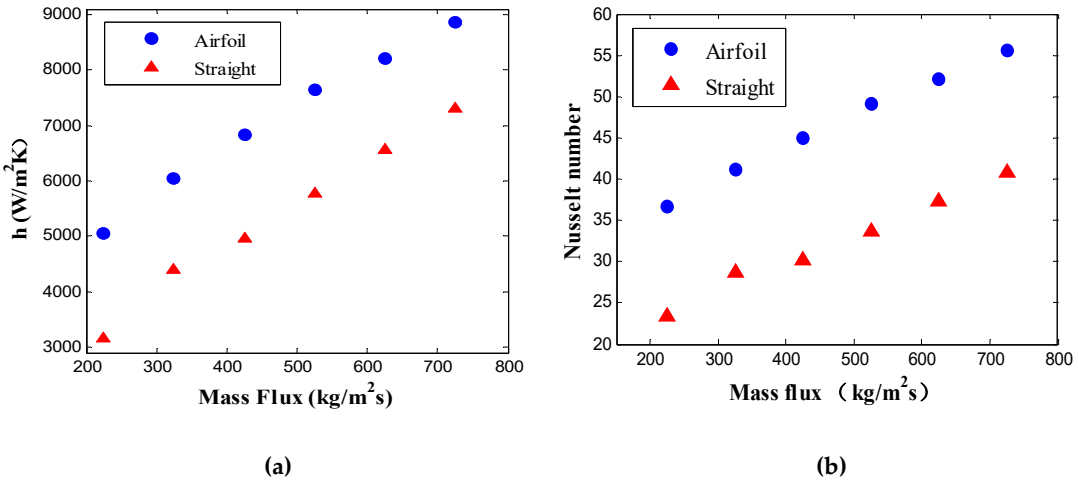


**Fig.14.** (a)Heat transfer coefficient h and (b) Nusselt number as a function of mass flux

To evaluate the effect of mass flux, six different mass fluxes were tested for straight channel and airfoil fin PCHEs. Fig.14 display the changes of heat transfer coefficient and Nusselt number at various mass fluxes respectively. Since the turbulence intensity of flow significantly increased with rising mass flux, the heat transfer coefficient and Nusselt number rapidly increased in both PCHEs. Also, the Nusselt number of airfoil fin PCHE exceeded that of straight channel PCHE. As we all know, the heat transfer and flow of a heat exchanger were affected by fins predominantly in two ways: giving rise to disturbance and enlarging heat transfer area. Therefore, airfoil fin PCHE showed better thermal performance than that of straight channel

Preprints (www.preprints.org) | NOT PEER-REVIEWED | Posted: 12 October 2017 doi:10.20944/preprints201710.0078.v1

Peer-reviewed version available at Energies 2017, 10, 1828; doi:10.3390/en10111828

PCHE at the same mass flux and hydraulic diameter. For example, when mass flux G = 425 kg/m²·s and G = 725 kg/m²·s, Nu values of airfoil fin PCHE were 1.48 and 1.36 times those of straight channel PCHE respectively.

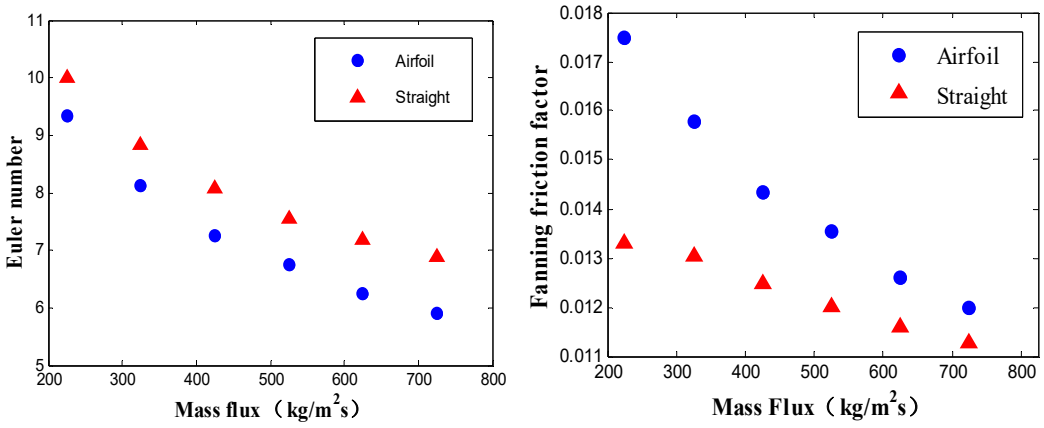


**Fig.15.** (a)Euler number and (b) fanning friction factor as a function of mass flux

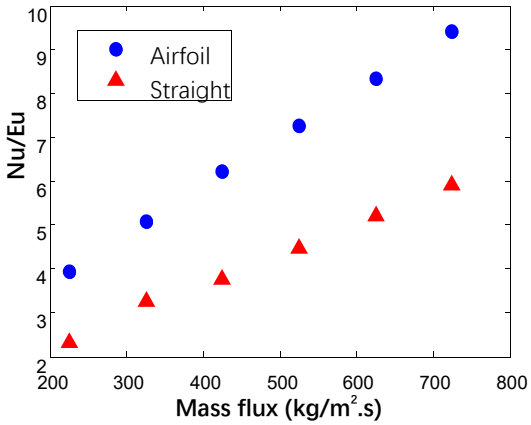


**Fig.16.** Nu/Eu as a function of mass flux

The effects of mass flux on the Euler number and Fanning friction factor of straight channel PCHE and airfoil fin PCHE were also assessed (Fig.15). The Euler number of straight channel PCHE surpassed that of airfoil fin PCHE. For example, when mass flux G = 425 kg/m²·s, the Euler number of airfoil fin PCHE was 89.7% of that of straight channel PCHE. Generally, pressure drop increases with rising mass flux. However, Figure 16 shows that the Euler number calculated by Eq. 12 decreases as the mass flux increases. According to this equation, the Euler number is proportional to pressure drop $\Delta P$ but inversely proportional to $v^2$. Obviously, the velocity of supercritical LNG rose with increasing mass flux, although it also raised the pressure drop. Nevertheless, $v^2$ exerted a stronger effect on Eu than on pressure drop, so the increase of mass flux led to decrease of the Euler number.

The heat transfer quantity and pressure drop, as the main indices of heat exchanger performance, were described as the Nusselt number and the Euler number herein, both helping to optimize the arrangement of airfoil fin. Generally, a specific objective function is used to verify an optimal design. The ratio of Nusselt number to Euler number, i.e. Nu/Eu, was employed as the objective function to evaluate the performance of heat exchanger. Fig.16

Preprints (www.preprints.org) | NOT PEER-REVIEWED | Posted: 12 October 2017 doi:10.20944/preprints201710.0078.v1

Peer-reviewed version available at Energies 2017, 10, 1828; doi:10.3390/en10111828

describes Nu/Eu as a function of mass flux. The minimum and maximum differences of Nu/Eu between straight channel PCHE and airfoil fin PCHE were 46.2% and 51.07% respectively. Evidently, airfoil fin PCHE had a better thermal-hydraulic performance, and the difference of Nu/Eu between airfoil fin and straight channel PCHEs increased with rising mass flux. Hence, fin arrangement is recommended for airfoil fin PCHE.

### *4.2 Effect of fin arrangement: staggered pitch ($L_s$)*

Fins affect flow and heat transfer primarily through their shapes and arrangements in PCHE. In this section, airfoil fins were arranged in parallel ($L_s$ = 0 mm) and staggered ($L_s$ = 1~4 mm) in the transverse direction of PCHE.

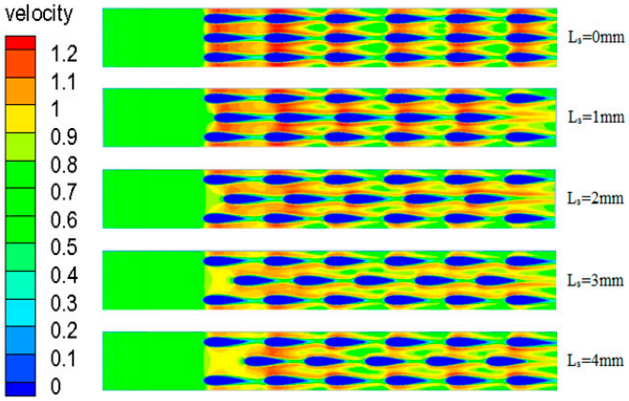


**Fig.17.** Velocity contour in PCHE with airfoil fins arranged at $L_v$ = 1.67 mm

In airfoil fin PCHE, the airfoil fins with wide head and narrow tail in favor of forming a much smoother flow channel when arranged in a staggered manner, and the vortex separation could also be prevented by the streamlined fins, which may result in a smaller flow resistance in staggered arrangement than that in parallel arrangement. Fig.17 depicts the velocity contour of supercritical LNG in airfoil fin PCHE arranged in parallel and staggered manners when the vertical pitch $L_v$ = 1.67 mm. In the start of heating, the velocities of fluid were quite uniform and small in both staggered and parallel arrangements. However, owing to continuous expansion and contraction in the sectional area of flow channel, the non-uniformity of velocity became obvious in parallel arrangement as the velocity increased in the flow direction. Therefore, a staggered arrangement of airfoil fins benefited the formation of smooth flow channel and the improvement of flow field uniformity.

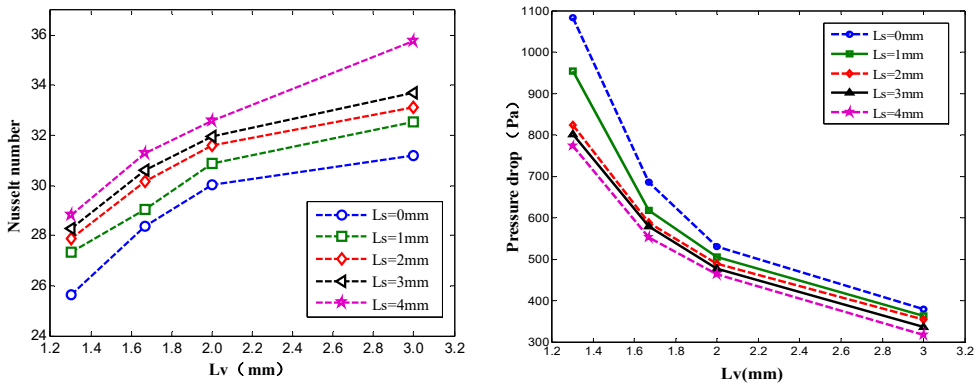


**(a)** **(b)**

Preprints (www.preprints.org) | NOT PEER-REVIEWED | Posted: 12 October 2017 doi:10.20944/preprints201710.0078.v1

Peer-reviewed version available at Energies 2017, 10, 1828; doi:10.3390/en10111828

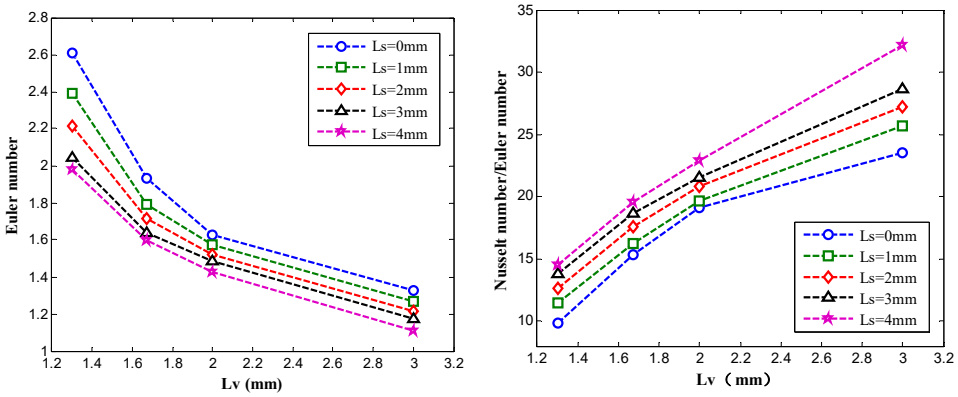


(c) (d)

**Fig.18.** Effect of $L_v$ on (a)Nusselt number ,(b)pressure drop, (c) Euler number and (d)Nu/Eu

Fig.18(a) shows the Nusselt numbers of airfoil fin PCHE in parallel and staggered arrangements. Clearly, the airfoil fins with staggered arrangement showed better thermal performance than that of the airfoil fins with parallel arrangement. However, at the same vertical pitch $L_v$, the Nusselt numbers of parallel and staggered arrangements were similar. The Nusselt number at $L_s$ = 0 mm differed from that at $L_s$ = 4 mm by 6.9% when the vertical number $L_v$ = 3 mm.

In addition, the flow resistance increased as the staggered pitch $L_s$ decreased. Fig.18(b) and Fig18.(c) present the pressure drop and Euler number with the staggered pitch ($L_s$) at different $L_v$ in airfoil fin PCHE. In Fig.18(c), the Euler number in staggered arrangement ($L_s$ = 1 mm) is smaller (a maximum decrease of 9.86%) than that in parallel arrangement ($L_s$ = 0 mm), with the difference enlarging as the staggered pitch ($L_s$) increases at the same vertical pitch $L_v$.

Fig.18(d) presents the dependence of Nu/Eu on $L_s$. Nu/Eu increased with rising staggered number $L_s$. $L_s$ = 0 mm had a lower Nu/Eu (about 27%) than that at $L_s$ = 4 mm, suggesting that $L_s$ = 4 mm had better heat transfer and pressure drop. Probably, pressure drop was more susceptible to $L_s$ than heat transfer. Collectively, staggered arrangement was superior to parallel arrangement in airfoil fin PCHE, manifested as reduced flow resistance and improved total thermal-hydraulic performance.

### *4.3 Effect of fin arrangement: vertical pitch ($L_v$)*

When $L_h$ (6 mm) is kept constant, $L_v$ directly determines the density of fins and the width of flow channel. Therefore, the effect of vertical separation distance ($L_v$) on the thermal-hydraulic performance of airfoil fin PCHE was assessed.

Preprints (www.preprints.org) | NOT PEER-REVIEWED | Posted: 12 October 2017 doi:10.20944/preprints201710.0078.v1

Peer-reviewed version available at Energies 2017, 10, 1828; doi:10.3390/en10111828

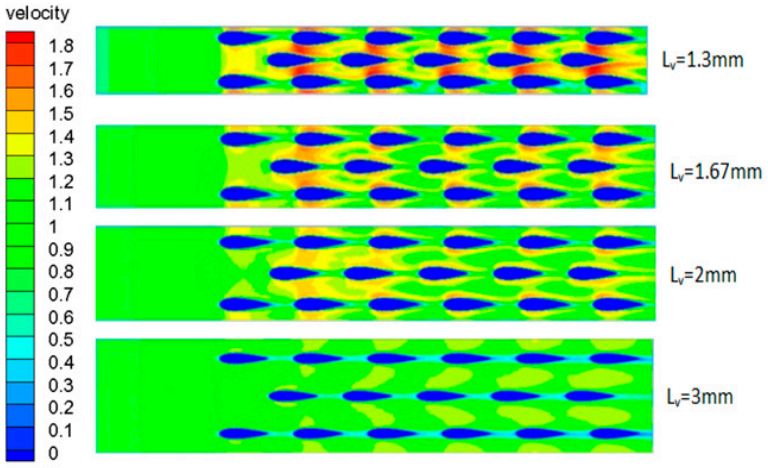


**Fig.19.** Velocity contour in PCHE with airfoil fins arranged at $L_s$ = 4 mm

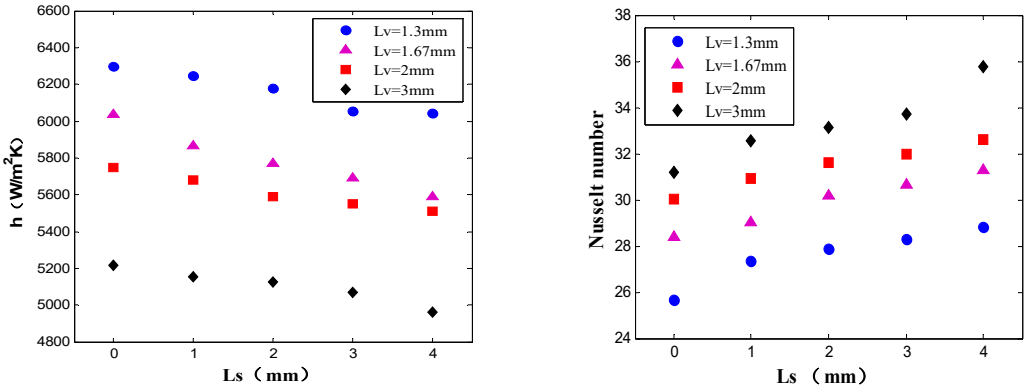


**(a)** **(b)**

**Fig.20.** Effect of $L_s$ on (a)heat transfer coefficient h and (b)Nusselt number

The velocity contours of supercritical LNG in airfoil fin PCHE arranged at different $L_v$ when the staggered pitch $L_s$ = 1.67 mm are presented in Fig.19. A smaller vertical pitch $L_v$ resulted in a higher velocity, thereby augmenting the flow resistance. In fact, a smaller $L_v$ led to a narrower sectional area of flow channel, so that the flow velocity increased with decreasing $L_v$ at the same mass flux. The maximum velocities of LNG in the narrowest sectional of flow channel were 1.35 m/s and 1.79 m/s in the airfoil fins with $L_s$ = 3 mm and $L_s$ = 1.3 mm respectively. Therefore, the turbulence intensity of fluid and the flow resistance were both enhanced locally.

Fig.20 exhibit the variations of heat transfer coefficient h and Nusselt number (Nu) with increasing fin distance ($L_v$) at different $L_s$ in airfoil fin PCHE. The convective heat transfer coefficient h decreased with rising $L_v$ at the same $L_s$, which may attributed to the decreased flow velocity. However, h and Nu changed oppositely with increasing $L_v$, mainly because the hydraulic diameter increased significantly faster than h decreased with rising $L_v$. For example, the hydraulic diameter at $L_v$ = 3 mm was nearly 2.7 times that at $L_v$ = 1.3 mm, and h at $L_v$ = 1.3 mm was 1.2 times that at $L_v$ = 1.3 mm when $L_s$ = 4 mm. Thus, the Nusselt number increased with rising $L_v$ of airfoil fins.

Preprints (www.preprints.org) | NOT PEER-REVIEWED | Posted: 12 October 2017 doi:10.20944/preprints201710.0078.v1

Peer-reviewed version available at Energies 2017, 10, 1828; doi:10.3390/en10111828

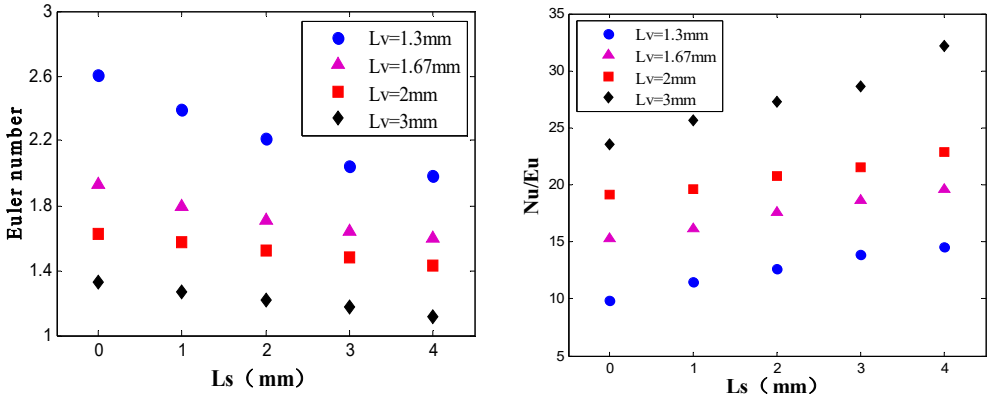


(a) (b)

**Fig.21.** Effect of $L_s$ on (a)Euler number and (b) Nu/Eu

Fig.21(a) shows the dependence of the Euler number on $L_v$. The total pressure drop decreased as $L_v$ increased, so the Euler number dropped more apparently with increasing $L_v$ at the same $L_s$. The Euler number at $L_v$ = 3 mm was only 56% of that at $L_v$ = 1.3 mm. Obviously, at the same $L_s$, reducing $L_v$ slightly facilitated heat transfer, though it also considerably elevated pressure drop.

As described in section 4.1, a specific objective function Nu/Eu was used to indicate the performance of airfoil fin PCHE. As exhibited in Fig.21(b), Nu/Eu noticeably rises as $L_v$ increases. Nu/Eu at $L_v$ = 3 mm is nearly 3 times and 1.7 times those at $L_v$ = 1.3 mm and $L_v$ = 2 mm respectively, indicating that a dense fin arrangement was conducive to increasing the heat transfer rate. Meanwhile, it was inevitably more difficult to overcome flow resistance. Accordingly, fins should be sparsely arranged in airfoil fin PCHE.

## 5. Conclusions

We here in aimed to clarify the thermal-hydraulic characteristics and optimal structure of a PCHE which supercritical LNG was used as the working fluid. The effects of channel shape and fin arrangements on the flow resistance and heat transfer in airfoil fin PCHE were numerically investigated as follows.

(1) The numerical model and methods were validated with the experimental data. Supercritical liquid nitrogen was used as a cold fluid for simulation and experiment. The SST model followed by the enhanced wall treatment method well predicted the outlet temperature and pressure drop of a single airfoil fin in PCHE. The error between the numerical and experimental data was within 14%, indicating the heat transfer and flow characteristics of supercritical LNG in airfoil fin PCHE could be reliably simulated by the model and method.

(2) As a new type of discontinuous fins, airfoil fins can boost the thermal-hydraulic performance compared with that of straight channel PCHE using supercritical LNG as the working fluid. The minimum and maximum differences of Nu/Eu between straight channel and airfoil fin PCHEs were 46.2% and 51.07% respectively. The convective heat transfer coefficient and pressure drop increased in both PCHEs with rising mass flux.

(3) Staggered fin arrangement was more beneficial to the thermal-hydraulic performance of airfoil fin PCHE than parallel fin arrangement using supercritical LNG as the working fluid.

423 At the same $L_v$ and $L_h$, airfoil fins arranged at $L_s$=4mm displayed better thermal-hydraulic
424 performance than those of the fins at other $L_s$.
425 (4) The velocity of supercritical LNG in airfoil fin channel increased along the channel
426 length and then plummeted with increasing $L_v$. The effect of vertical number $L_v$ on the thermal-
427 hydraulic performance of airfoil fin PCHE was more evident than that of staggered pitch $L_s$.
428 Based on a comprehensive analysis of heat transfer coefficient and pressure drop, a sparser
429 staggered arrangement of fins can enhance the thermal-hydraulic performance of airfoil fin
430 PCHE.
431

**Acknowledgement :** The authors gratefully acknowledge that this work was Jiangsu marine and fishery science and technology innovation and extension project(HY2017-8) and Zhenjiang funds for the key research and development project(GY2016002-1)

**Nomenclature**

| | |
|---|---|
| f | Fanning factor |
| v | Velocity (m/s) |
| Re | Reynolds number |
| h | Convective heat transfer coefficient (W/m²·K) |
| Nu | Nusselt number |
| $C_p$ | Specific heat (kJ/kg·K) |
| $D_h$ | Hydraulic diameter (mm) |
| $q_m$ | Mass flow rate (kg/s) |
| u | Velocity (m/s) |
| q'' | Heat flux (W/m²) |
| G | Mass flux (kg/m²·s) |
| $L_v$ | The pitch between one airfoil head and adjacent row in the vertical direction (mm) |
| $L_s$ | The pitch of the staggered arrangement (mm) |
| $L_h$ | The pitch between one airfoil head and adjacent airfoil head in a row (mm) |
| ΔP | Pressure drop (Pa) |
| $\Delta p_{fric}$ | Pressure drop due to friction (Pa) |
| $\Delta p_{acc}$ | Pressure drop due to acceleration (Pa) |
| $\rho_{in}$ | Density at the inlet of the channel (kg/m³) |
| $\rho_{out}$ | Density at the outlet of the channel (kg/m³) |
| $\tau_w$ | Shear stress at the wall (Pa) |
| | Greek symbols |
| μ | Viscosity [Pa·s] |
| ρ | Density [kg/m³] |
| λ | Thermal conductivity [W/m²·K] |
| Subscript | |
| w | Wall |
| b | Bulk mean |
| acc | Acceleration |
| fric | Friction |
| v | Vertical |
| s | Staggered |
| h | Horizontal |
| in | Inlet |
| out | Outlet |

## References

[1] A. Yousefi, M. Birouk. Investigation of natural gas energy fraction and injection timing on the performance and emissions of a dual-fuel engine with pre-combustion chamber under low engine load. Applied Energy 189(2017):492-505.

[2] T. N. Pham,et al. Enhancement of single mixed refrigerant natural gas liquefaction process through process knowledge inspired optimization and modification. Applied Thermal Engineering, 110(2017):1230-1239.

[3] Pu Liang, et al. Thermal performance analysis of intermediate fluid vaporizer for liquefied natural gas. Applied Thermal Engineering, 65.1-2(2014):564–574.

[4] Ting Wang, Boqiang Lin. China's natural gas consumption peak and factors analysis: a regional perspective. Journal of Cleaner Production,142(2017):548-564.

[5] Jie Pan, Ran Li, Tao Lv, Gang Wu, Zhian Deng. Thermal performance calculation and analysis of heat transfer tube in super open rack vaporizer.93(2016):27-35.

[6] Shanshan Liu, Wenling Jiao, Haichao Wang. Three-dimensional numerical analysis of the coupled heat transfer performance of LNG ambient air vaporizer. Renewable Energy,87(2016):1105-1112.

[7] Chang-Liang Han, Jing-Jie Ren, Yan-Qing Wang, Wen-Ping Dong, Ming-Shu Bi. Experimental investigation on fluid flow and heat transfer characteristics of a submerged combustion vaporizer.Applied thermal Engineering,113(2017):529-536.

[8] Liang Pu, Zhiguo Qu, Yuheng Bai, Di Qi, Kun Song, Peng Yi. Thermal performance analysis of intermediate fluid vaporizer for liquefied natural gas. Applied Thermal Engineering,65(2014):564-574.

[9] Su-Jong Yoon, Piyush Sabharwall, Eung-Soo Kim. Numerical study on crossflow printed circuit heat exchanger for advanced small modular reactors. 70(2014):250-263.

[10] N.Tsuzuki, Y.Kato, T.Ishiduka. High Performance Printed Circuit Heat Exchanger [J].Applied Thermal Engineering. 27(2007):1702-1707.

[11]In Hun Kim, Hee Cheon No. Thermal hydraulic performance analysis of a printed circuit heat exchanger using a helium–water test loop and numerical simulations. Applied Thermal Engineering. 31(2011):4064-4073.

[12] I.H. Kim, H.C. No, J.I. Lee, B.G. Jeon, Thermal hydraulic performance analysis of the printed circuit heat exchanger using a helium test facility and CFD simulations, Nuclear Engineering &Design. 239 (2009) :2399-2408.

[13] In Hun Kim, Hee Cheon No. Physical model development and optimal design of PCHE for intermediate heat exchangers in HTGRs. Nuclear Engineering and Design, 243(2012):243-250.

[14] Mylavarapu SK, Sun XD, Christensen RN, Unocic RR, Glosup RE, Patterson MW.Fabrication and design aspects of high-temperature compact diffusion bonded heat exchangers. Nuclear Engineering and Design.249(2012): 49–56.

[15] M.V.V. Mortean, K.V. Paiva, M.B.H. Mantelli. Diffusion bonded cross-flow compact heat exchangers: Theoretical predictions and experiments[J]. International Journal of Thermal Sciences. 2016(110):285-298.

[16] K. In Hun, Z. Xiaoqin, R. Christensen, et al. Disign study and cost assessment of straighe, zigzag, S-shape,and OSF PCHEs for a FLiNaK-SCO2 Secondary Heat Exchanger in FHRs [J]. Annals of Nuclear Energy. 2016 (94): 129-137.

[17] Natesan K, Moisseytsev A, Majumdar S. Preliminary issues associated with the next generation nuclear plant intermediate heat exchanger design. J Nucl Mater 2009;392(2):307–15.

[18] S. B. Hosseini, R. H. Khoshkhoo, S.M. Javadi Malabad. Experimental and numerical investigation on particle deposition in a compact heat exchanger [J]. Applied Thermal Engineering. 2017(115):406-417.

[19] G. Starace, M. Fiorentino, M.P. Longo, et al. A hybrid method for the cross flow compact heat exchangers design[J]. Applied Thermal Engineering. 2017(111):1129-1142.

[20] M.Y.Park, M.S.Song, E. S.Kim. Development of tritium permeation model for Printed Circuit Heat Exchanger[J]. Annals of nuclear energy. 2016(98):166-177.

[21] S.Baek, J.Kim, S.Jeong, et al. Development of highly effective cryogenic printed circuit heat exchanger (PCHE) with low axial conduction [J]. Cryogenics 52. 7-9(2012):366-374.

[22] Kim, In. Hun., & N. O. Hee Cheon. Thermal–hydraulic physical models for a printed circuit heat exchanger covering he, he–co2 mixture, and water fluids using experimental data and cfd. Experimental Thermal & Fluid Science, 48. 7(2013): 213-221.

[23] Lee. Sang-Moon, Kim wang-Yong. Comparative study on performance of a zigzag printed circuit heat exchanger with various channel shapes and configurations [J].Heat Mass Transfer. 49. 7(2013): 1021-1028.

[24] Lee.Sang-Moon, Kim wang-Yong. Multi-objective optimization of arc-shaped ribs in the channels of a printed circuit heat exchanger [J]. International Journal of Thermal Sciences, 94(2015):1-8.

[25] S.K. Mylavarapu, X.D. Sun, R.E. Glosup, R.N. Christensen, M.W. Patterson. Thermal hydraulic performance testing of printed circuit heat exchangers in a high-temperature helium test facility, Applied Thermal Engeering. 65 (2014) :605-614.

[26] T. Ma, L. Li, X.Y. Xu, Y.T. Chen, Q.W. Wang. Study on local thermal-hydraulic performance and optimization of zigzag-type printed circuit heat exchanger at high temperature. Energy Conversion and Management. 104 (2015):55-66.

[27] J. Figley, X. Sun, S.K. Mylavarapu, B. Hajek, Numerical study on thermal hydraulic performance of a printed circuit heat exchanger, Prog. Nucl. Energy .68 (2013) :89–96.

[28] A.M.Aneesh, A.Sharma, A.Srivastava, et al. Thermal-hydraulic characteristics and performance of 3D straight channel based printed circuit heat exchanger[J]. Applied Thermal Engineering. 98 (2016):474-482.

[29] H.K. Hamid, A.M. Aneesh, S. Autl, et al., Thermal hydraulic characteristics and performance of 3D wavy channel based printed circuit heat exchanger. 87(2015):519-528.

[30] T.L. Ngo, Y. Kato, K. Nikitin, et al., New printed circuit heat exchanger with S-shaped fins for hot water supplier, Experimental Thermal & Fluid Science. 30. 8(2006):811–819.

[31] D.E. Kim, M.H. Kim, J.E. Cha, S.O. Kim, Numerical investigation on thermal-hydraulic performance of new printed circuit heat exchanger model, Nuclear Engineering and Design. 238 (2008) :3269-3276.

[32] X. Xiangyang, M.Ting, L.Lei, et al. Optimization of fin arrangement and channel configuration in an airfoil fin PCHE for supercritical CO2 cycle [J]. Applied Thermal Engineering. 113(2014):867-875.

[33] Chang-Liang Han, Jing-Jie Ren, Wen-Ping Dong, Ming-Shu Bi. Numerical investigation of supercritical LNG convective heat transfer in a horizontal serpentine tube. Cryogenics. 78(2016):1-13.

[34] Y. Yoon, Bae. A new formulation of variable turbulent prandtl number for heat transfer to supercritical fluids [J]. 92 (2016):792-806.

[35] S.Jeon, Y.Baik, C.Byon, et al. Thermal performance of heterogeneous PCHE for supercritical CO2 energy cycle [J]. International Journal of Heat and Mass Transfer. 102(2016):867-876.

[36] Kruizenga A, Anderson M, Fatima R, Corradini M, Towne A, Ranjan D. Heat transfer of supercritical

carbon dioxide in printed circuit heat exchanger geometries. Journal of thermal Science and Engineering Application. 3(2011) 031002:1-8.

[37] Tae Ho Kim, Jin Gyu Kwon, Sung Ho Yoon, Hyun Sun Park, Moo Hwan Kim, Jae Eun Cha. Numerical analysis of air-foil shaped fin performance in printed circuit heat exchanger in a supercritical carbon dioxide power cycle. Nuclear Engineering and Design. 288(2015):110-118.